Available online at www.sciencedirect.com

SCIENCE DIRECT®

Tectonophysics 387 (2004) 65–79

TECTONOPHYSICS

www.elsevier.com/locate/tecto

A study of the 2 December 2002 (**M**5.5) Vartholomio (western Peloponnese, Greece) earthquake and of its largest aftershocks

Z. Roumelioti[a], Ch. Benetatos[a], A. Kiratzi[a,*], G. Stavrakakis[b], N. Melis[b]

[a]*Department of Geophysics, Aristotle University of Thessaloniki, 54124 Thessaloniki, Greece*
[b]*Geodynamic Institute, National Observatory of Athens, P.O. Box 20048, 11810 Athens, Greece*

Received 7 October 2003; accepted 8 June 2004
Available online 18 August 2004

Abstract

Broadband data from the Greek National Seismological Network are used to study the moderate size (**M**5.5) earthquake, which occurred on 2 December 2002 near the town of Vartholomio, in western Peloponnese (Greece). Time domain moment tensor inversion applied to retrieve the focal mechanism of the mainshock and of three of the larger aftershocks of the sequence, revealed almost pure strike-slip faulting along NW–SE or NE–SW trending nodal planes. The relative source time functions for the mainshock, obtained from an empirical Green's function analysis, do not reveal any clear directivity to any of the stations. A careful observer might suggest directivity towards NW, if any. Optimum values are 0.4 s for the rise time and 2.7 km/s for the rupture velocity. The spatial and temporal distribution of fault slip showed that the major part of the resolved slip occurred beneath the mainshock's epicenter, ~20 km underneath the western coast of Peloponnese. This probably accounts for the considerable damage observed to the nearby towns. The resolution between the two nodal planes does not permit an identification of the fault plane; however the statistics on the slip distribution model, the preliminary analysis of aftershock locations and macroseismic data favour the NW–SE trending plane as the fault plane, which is connected with sinistral strike-slip motions. These are the first implications for sinistral strike-slip motions in this area and more data are needed in the future to get more reliable resolution of the motions.

Keywords: Vartholomio earthquake; Aegean; Greece; Slip distribution; Source time function; Focal mechanism

1. Introduction

On 2 December, 2002 a moderate size (of moment magnitude **M**5.5) earthquake hit western Peloponnese (Greece). Most of the damage was reported in Vartholomio, a town located about 9 km north–northeast of the epicenter. At least 17 people were injured when a rockslide near Megalopolis caused a train to derail. At least eight houses were destroyed and 100 were damaged, and a monastery partially collapsed in the Vartholomio area. The earthquake was strongly felt on Zakyn-

* Corresponding author. Tel.: +30 2310 998486; fax: +30 2310 998528.
E-mail address: Kiratzi@geo.auth.gr (A. Kiratzi).

0040-1951/$ - see front matter © 2004 Elsevier B.V. All rights reserved.
doi:10.1016/j.tecto.2004.06.008

thos Island as well as in Arcadia and Corinth Provinces.

The earthquake, even though moderate in size, is of great interest and importance as it occurred in an area characterized by high levels of seismic hazard. The 2002 Vartholomio sequence provided a plethora of broadband waveforms that can be incorporated in modern techniques to gain insight into the source process of earthquakes in this area, as well as better knowledge of the general seismotectonic regime.

In this work we apply time domain moment tensor inversion to determine the focal mechanism of the mainshock and of the larger aftershocks, as well as the distribution of slip during the mainshock using a source time function inversion scheme. Special effort is given in identifying the causative fault by combining results from independent analyses.

2. Seismotectonic setting

As part of the broader Aegean area, western Greece consists a seismotectonically complex area of rapid and intense deformation. The predominant features of the present seismotectonic setting of this area result from the net effect of the relative motions of the Aegean plate, the African plate and the Apulian platform (Fig. 1). The Cephalonia–Lefkada transform fault, in the area of the Ionian Islands, marks the transition zone between the continental collision of the Apulia platform and Eurasia to the north and the Hellenic subduction to the south. In general, the Aegean plate is subject to large-scale extension, which is evidenced by its southwestward motion relative to Europe (e.g. McKenzie, 1972; Le Pichon et al., 1995; McClusky et al., 2000), whereas compression is observed along the Hellenic subduction zone.

Kiratzi and Louvari (2003) compiled a database, a part of which includes all known focal mechanisms of earthquakes in western Greece and they showed the domination of strike-slip motions in the area between the Ionian Islands (Cephalonia–Lefkada transform fault) and western Peloponnese (Fig. 1). Although the character of faulting around the Ionian Islands is very well known to be dextral (Louvari et al., 1999 and references therein; Kiratzi and Louvari, 2003; Papadopoulos et al., 2003; Benetatos et al., submitted for publication), the sense of motion on the strike-slip faults of western Peloponnese has not been evidenced so far. Therefore, one of the aims of the present study is to gain more insight into the kinematics of the deformation within the wider seismotectonic setting of the 2002 Vartholomio earthquake.

3. Data

Data used consist of broadband waveforms recorded by the Greek National Broadband Network (Fig. 2), operated by the Geodynamic Institute of the National Observatory of Athens since 1999. The stations of the network are equipped with Lennartz LE-3D/20s, three-component sensors installed all over Greece.

A shortcoming of the examined earthquake is the fact that its location is at the westernmost part of the network (Fig. 2) and as a result there is a significant azimuthal gap of about 180° for which we have no data. This distribution can affect the results of the slip study by shifting the relative positions of possible discrete areas of slip concentration. Nevertheless, it has been previously shown that even with station coverage of 180° it is possible to resolve the rough characteristics of the slip distribution pattern (Antolik, 1996).

4. Time domain moment tensor inversion

4.1. Method

Inversion for the seismic moment tensor was done following the approach of Dreger and Helmberger (1990, 1993), using broadband waveform data recorded at regional distances. The employed inversion method is capable of revealing the seismic moment tensor of earthquakes of local magnitudes as low as **M**3.5 (Pasyanos et al., 1996). A single three-component station can often resolve the moment-tensor parameters, although incorporation of a larger number of stations improves the stability of the results (Dreger and Helmberger, 1991).

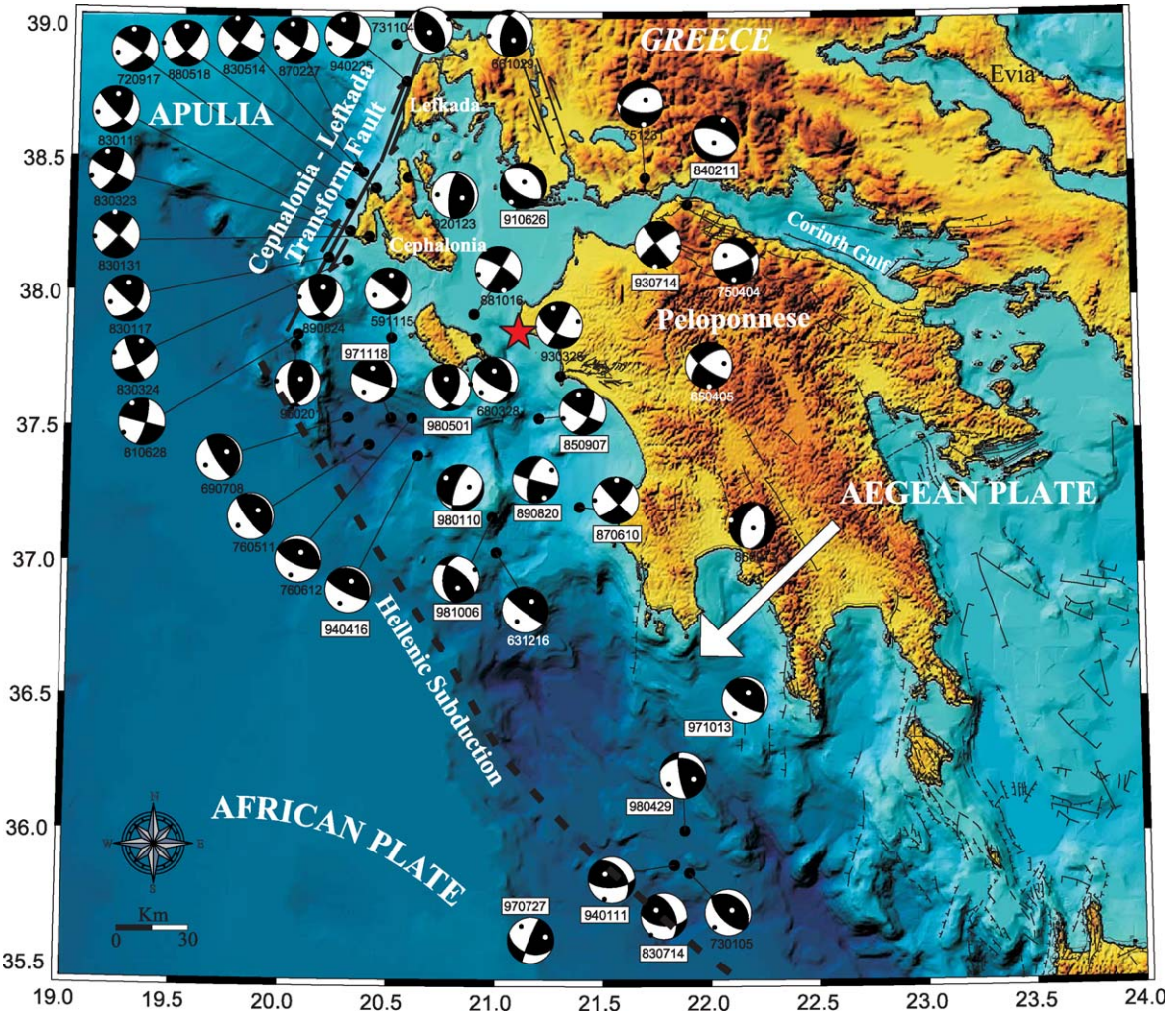

Fig. 1. Previously published focal mechanisms of earthquakes in western Greece (the date of occurrence is shown next to each beachball). The arrows indicate the motion of the plates relative to Europe and the star symbol corresponds to the epicentre of the 2002 Vartholomio mainshock. Strike-slip events are related to the Cephalonia–Lefkada transform fault and are also distributed along the western coast of Peloponnese, whereas thrust events are observed along the Hellenic subduction zone (figure modified after Kiratzi and Louvari, 2003).

The general representation of the seismic source is simplified by considering a point source both in space and time:

$$U_n(x,t) = M_{ij} G_{ni,j}(x,z,t,) \quad (1)$$

where U_n is the nth observed component of displacement, $G_{ni,j}$ is the nth component Green's function for specific force-couple orientations, x corresponds to the source-station distance, z is the source depth and M_{ij} is the scalar seismic moment tensor. The general force-couples for a deviatoric moment tensor may be represented by three fundamental faults, namely a vertical strike-slip, a vertical dip-slip, and a 45° dip-slip (Jost and Herrmann, 1989). In order to apply the methodology, the following assumptions are made: the crustal model is sufficiently well known to explain the low frequency part of the regionally recorded waveforms, event location can be represented by the high frequency hypocentral location and the source time history is synchronous for all moment tensor elements.

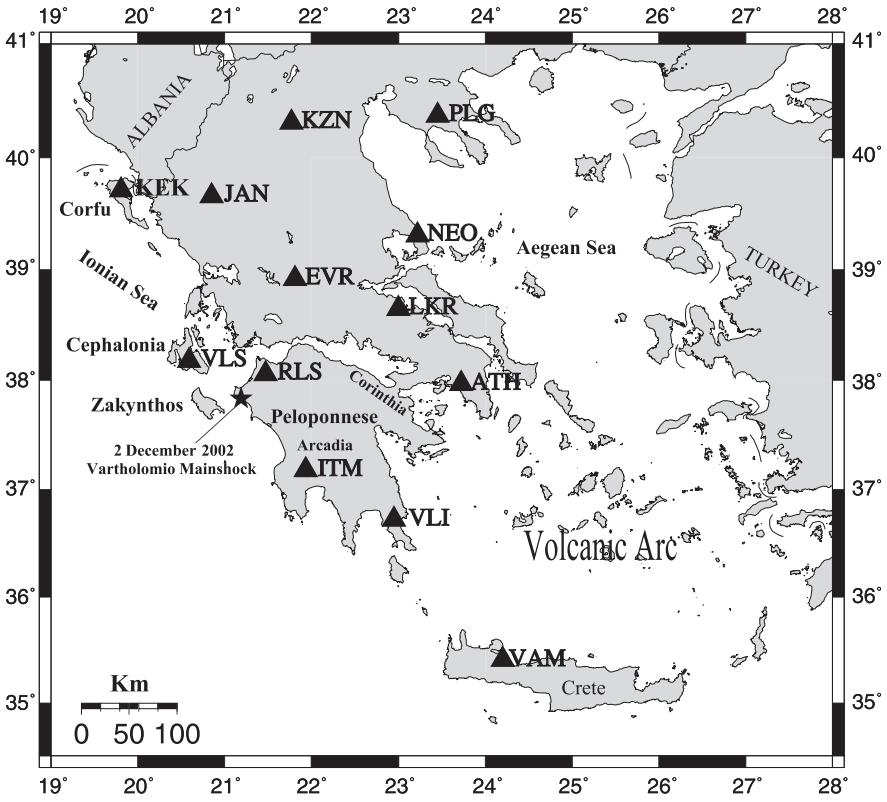

Fig. 2. Regional map showing the locations of the broadband stations used in the present study (triangles) with respect to the 2002 Vartholomio mainshock epicentre (star).

Eq. (1) is solved using linear least squares for a given source depth. The inversion yields the M_{ij}, which is decomposed into the scalar seismic moment, a double-couple (DC) moment tensor and a compensated linear vector dipole moment tensor (CLVD). The basic method and decomposition of the seismic moment tensor is described in Jost and Herrmann (1989). The optimum hypocentral depth is found by iteration and evaluating an objective function (f) that depends upon the RMS of the difference of the observed waveforms (data) and the synthetic waveforms (synth), modulated by the percent double couple (Pdc):

$$f = \frac{\mathrm{RMS}(\mathrm{data} - \mathrm{synth})}{\mathrm{Pdc}} \tag{2}$$

Another measure that is used is the variance reduction (VR):

$$\mathrm{VR} = 1.0 - \frac{\int [\mathrm{data} - \mathrm{synth}]^2 \mathrm{d}t}{\int [\mathrm{data}]^2 \mathrm{d}t} \tag{3}$$

A successful application of the method results in small values of the objective function (f) and large values of variance reduction (VR), indicating that both the fit between the observed and synthetic waveforms and the percent of double couple are large.

4.2. Application results

The focal mechanisms of the Vartholomio mainshock and few of its largest aftershocks were investigated using the time domain moment tensor inversion technique and broadband data from the

Table 1
Velocity model (Tselentis and Zahradnik, 2000) adopted for the calculation of theoretical Green's functions in the time-domain moment tensor inversion method

Depth (km)	V_P (km/s)	Q
0.0	2.67	300
1.0	4.45	300
2.0	5.70	300
5.0	6.00	300
18.0	6.40	300
39.0	7.90	1000

V_P/V_S was assumed to be equal to 1.78.

Greek national network. The successful implementation of the method requires an appropriate 1D velocity model that could adequately explain the geological structure between the recording stations and the earthquakes to be modelled. For this purpose we tested two 1D velocity models routinely used in Greece. The first model has been proposed by Panagiotopoulos et al. (1985) and is used for routine earthquake locations by the Geophysical Laboratory of the Aristotle University of Thessaloniki. The second model has been empirically determined based on regional broadband waveform modeling (Tselentis and Zahradnik, 2000). The two models had similar performance in the investigated frequency ranges and the results presented in this study are those estimated using the latter model, which is presented in Table 1.

The selected 1D model was used as input in the frequency wavenumber integration code (FKRPROG) developed by Saikia (1994) in order to compute synthetic Green's functions for the examined hypocenter-station distances. The resulting theoretical Green's functions were then used in the time domain moment tensor inversion code (TDMT_INVC, Dreger, 2002) to derive the focal mechanisms of the examined events.

The three component broadband seismograms were cut into time segments of 5 min of raw data, in order for the signal to be long enough to ensure resolution of the low frequencies. Then, the selected data were corrected for the instrument response, integrated to displacement, filtered in the frequency range 0.05–0.08 Hz and resampled at 1 sample per second. The type of our recording instruments imposes the lower limit of the selected frequency range and the higher limit was based on tests performed on the present data set, as well as on previous studies (Zahradnik, 2001; Benetatos et al., 2002).

We used the time domain moment tensor inversion technique to estimate the focal mechanism of the Vartholomio mainshock (**M**5.5) and four of its largest aftershocks. The parameters of the modelled earthquakes are listed in Table 2. The employed 1D velocity model adequately explained the recorded low frequencies at five stations of the regional network, namely RLS, VLS, ITM, VLI, and KEK (Fig. 2). These five stations are located at epicentral distances ranging from 44 km to 240 km and were used to model the 2002 Vartholomio mainshock. All smaller events were modelled using fewer stations due to their smaller signal-to-noise ratio at more distant stations. Nevertheless, a minimum of two stations was set in all cases during the inversion procedure.

The optimum depth for each one of the studied earthquakes was found iteratively by examining the overall variance and the variance reduction, that the

Table 2
Source parameters of the 2 December 2002 Vartholomio earthquake, of the event used as eGf and of the three larger aftershocks derived from time domain moment tensor inversion

Earthquake	Date (yymmdd)	Time	Lat. °N	Lon. °E	**M**	Depth (Km)	Plane 1			Plane 2			No. of stations (used in the inversion)
							Azimuth (°)	Dip (°)	Rake (°)	Azimuth (°)	Dip (°)	Rake (°)	
Mainshock	021202	04:58:56	37.83	21.12	5.5	17	50	68	−166	315	77	−22	5
Aftershock 1	021203	00:38:57	37.82	21.12	4.1	17	44	79	−173	312	83	−11	4
Aftershock 2	021213	01:19:47	37.83	21.09	4.0	8	47	58	−166	309	78	−33	4
Aftershock 3	021204	22:35:15	37.84	21.13	3.8	9	80	86	63	342	27	171	3
eGf	020930	19:58:12	37.83	21.12	4.1	16	32	75	−165	299	81	−10	2

Epicentral coordinates were derived after relocating the sequence epicenters using the HypoDD code of Waldhauser and Ellsworth (2000).

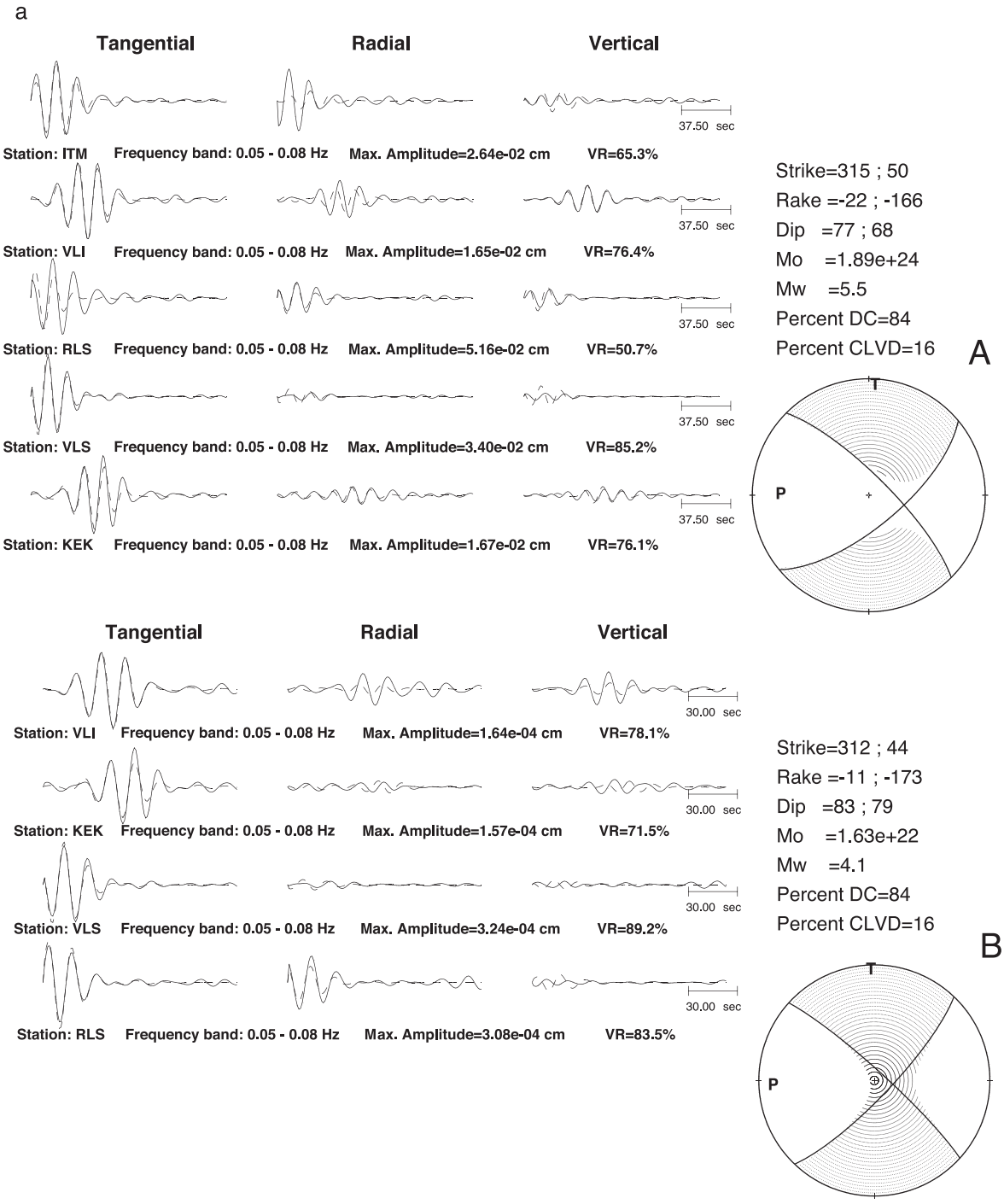

Fig. 3. (a) Time domain moment tensor inversion results for the earthquakes listed in Table 2: (A) the 2002 Vartholomio mainshock, (B) Aftershock 1. The observed tangential, radial and vertical components (solid lines) are compared with the synthetics (dashed lines) at each one of the stations used in the inversion. At the same figures the results of the inversion routine along with the focal mechanism parameters are shown on the right. Seismic moment is given in dyn-cm. (b) As in (a) for: (C) aftershock 2, (D) aftershock 3 and (E) the eGf.

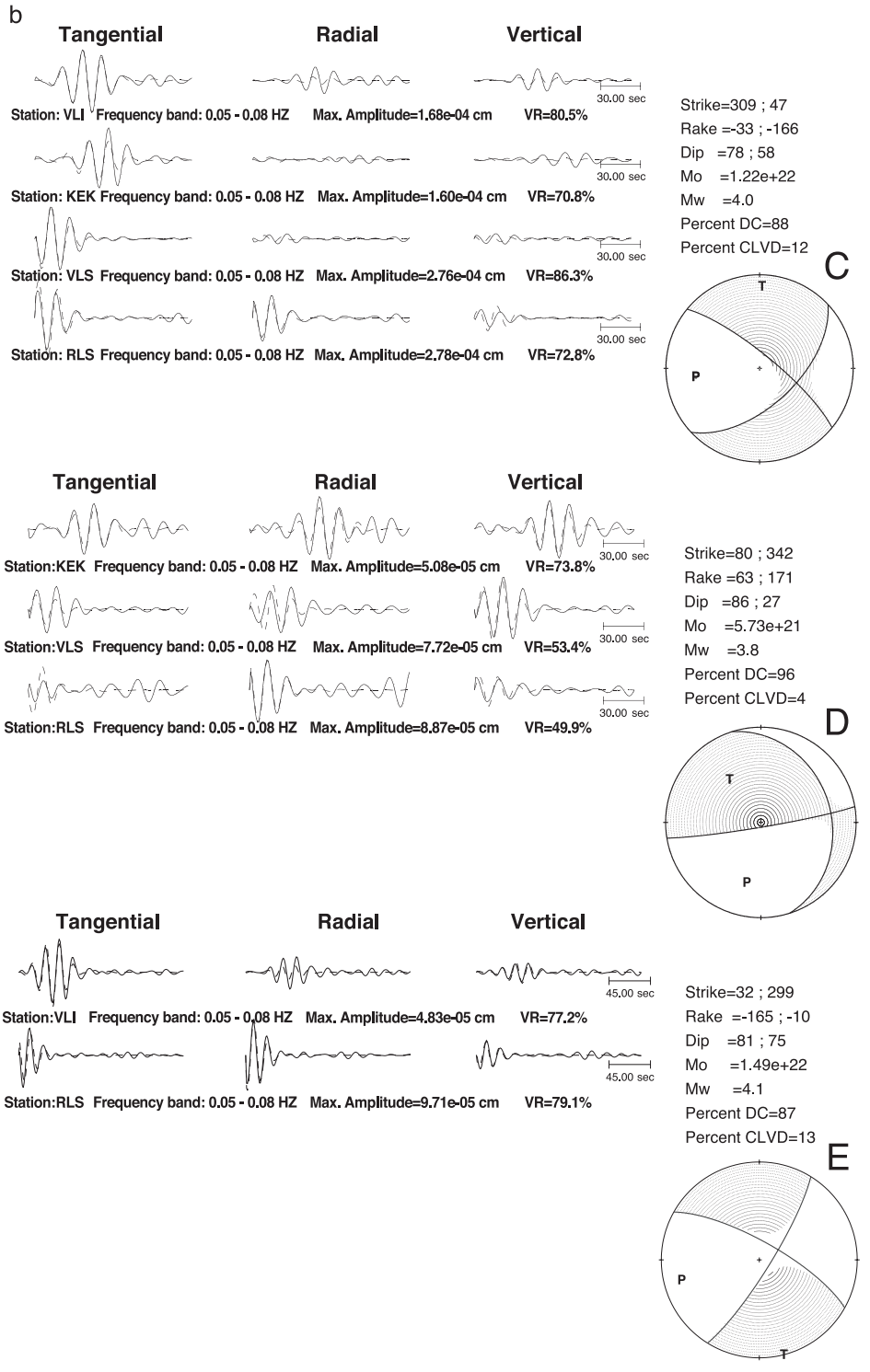

Fig. 3 (*continued*).

inversion routine was returning at each run, and the percent double couple of the focal mechanism. We tested depth values spanning the range 3–25 km (using a step of 1 km), which covers the usually observed focal depths of shallow earthquakes in Greece. The focal mechanism solutions proved to be very stable during the tests at different depths, although in many cases it was necessary to manually align the synthetics relative to the observed waveforms in order to achieve the best fit between them. A posteriori tests revealed that for some earthquakes we could resolve a reliable focal mechanism by inverting data from only one station, although in most cases a minimum number of two stations was required to achieve stable results. This result reflects the variant performance of the employed 1D velocity model along different wave paths. The results of the time domain moment tensor inversion are presented in Fig. 3(a, b) and Table 2, whereas in Table 3 we compare the source parameters of the mainshock computed in the frame of this study with corresponding parameters computed by other institutes. Four out of the five computed moment tensors, including the one of the mainshock, imply almost pure strike-slip faulting along either northwest–southeast or northeast–southwest trending planes. On the other hand, the moment tensor of the smallest aftershock analysed (Fig. 3b(D)) implies reverse faulting with a significant strike-slip component, along north–south or east–west trending planes. As discussed later, this aftershock may be related to a secondary structure, which was activated after the mainshock rupture. Variance reduction values in all moment tensor estimates vary from approximately 50% (e.g. station RLS in Fig. 3a(A)) up to almost 90% (e.g. station VLS in Fig. 3a(B)), reflecting a satisfactory fit between observed and synthetic waveforms.

Table 3
Source parameters of the 2 December 2002 Vartholomio earthquake, as estimated by different institutes

Institute	Strike	Dip	Rake	Depth (km)	Seismic moment (Nt · m)
HARVARD	36	56	−160	15	3.42×10^{17}
Swiss (ETH)	36	77	−167	27	4.55×10^{17}
MEDNET	33	81	−175	23	2.90×10^{17}
Present article	50	68	−166	17	1.89×10^{17}

5. Source time function inversion

5.1. Method

The slip distribution of the 2002 Vartholomio mainshock was retrieved using an earthquake source inversion method, introduced by Mori and Hartzell (1990) for local earthquakes and later extended to regional distances by Dreger (1994). In this method, propagation path and radiation pattern effects in the regional records of the examined event are removed by using a nearby smaller event, with similar focal mechanism, as empirical Green's function (Hartzell, 1978). In other words, the selected small event is considered to be a point source in both space and time. The waveforms of the smaller event are deconvolved from the corresponding waveforms of the larger event and the output of this operation are the source time functions of the large event, which are relative to the actual source time functions of the small event. Therefore the successful application of the method depends on the selection of the event to be used as empirical Green's function, which must be small enough to ensure the validity of the point-source assumption.

In the applied method, the entire waveforms of both the large and the small event are used under the assumption that they are dominated by the S-wave phases. This assumption has been proven to give reliable results when working with regional waveforms (Dreger, 1994) and especially at distances smaller than 200 km. This is an advantage of the method since isolation of different phases at regional distances is a rather difficult and sometimes unfeasible task.

A general mathematical representation of the method in the frequency domain, at distance r and azimuth ϕ from the seismogenic area is:

$$\frac{U(\omega)}{u(\omega)} = \frac{\dot{M}(\omega)G(\omega,r,\phi)RI(\omega)}{\delta(\omega)G(\omega,r,\phi)RI(\omega)} = \dot{M}(\omega) \qquad (4)$$

where U and u are the far-field displacement spectra of the records of the large and the small event, respectively, $\dot{M}$ is the moment rate function of the large event and δ the corresponding function of the small event which is considered to be a delta function (point-source assumption), G is the Green's function

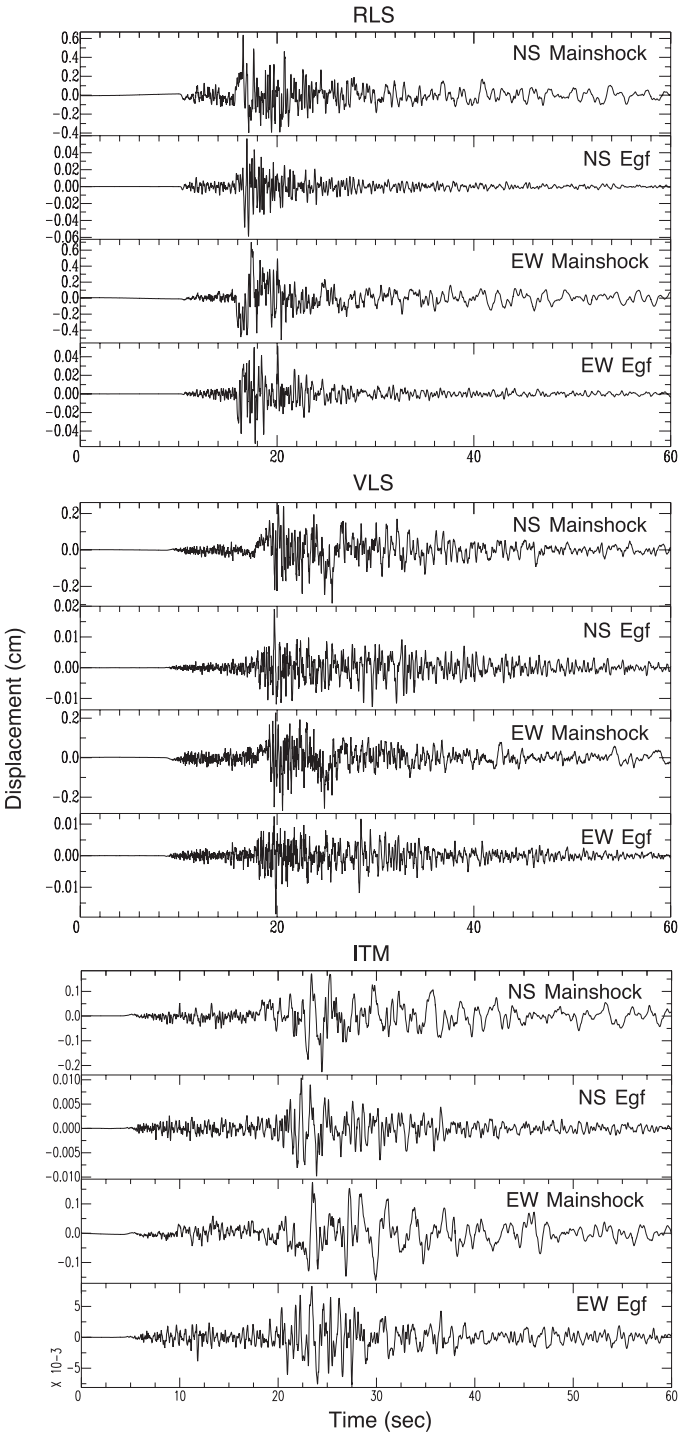

Fig. 4. Comparison of the displacement waveforms (North–South and East–West components), at three selected stations, for the 2002 Vartholomio mainshock with those of the employed empirical Green's function. The similarity is very good.

response of the medium along the wave path, which includes the effects of attenuation and geometrical spreading, R is the radiation pattern factor and I is the response of the recording instrument. In the above equation, the propagation path (G), recording instrument (I) and radiation pattern (R) effects are considered to be the same for both events. Therefore, the division of the two displacement spectra gives the moment rate function, $\dot{M}$, of the large event. The source time function (STF) is then computed by inverse fast Fourier transformation.

The aforementioned procedure is repeated for each one of the available regional broadband waveforms. Prior to the inversion, the estimated STFs are normalized to unit area. This is done to avoid problems in the absolute amplitudes due to differences in the radiation patterns of the eGf and mainshock, and to ensure that all STFs used integrate to the appropriate scalar seismic moment.

The following step involves the inversion of the STFs, which are estimated as previously described. The employed inversion technique (Mori and Hartzell, 1990) is based on the assumption that the variations in STF shape can be mapped onto the spatial and temporal slip history of the event. The source is parameterized through a radially propagating rupture front, which expands with a constant rupture velocity. Slip is confined to one of the nodal planes indicated by the focal mechanism of the event. Then the inverse method fits the STF of the examined event by summing contributions from different subfaults, taking into account the time delay due to wave propagation and to the propagation of the rupture front, with respect to the hypocenter. Distances to the different subfaults are estimated using a half space ray trajectory approximation. The contribution from each subfault can take the form of several synthetic time functions. Here, the subfault STFs have the form of boxcar functions. The optimal values for the fault orientation, the rupture velocity and the dislocation rise time are found by performing a series of inversions testing the parameter space.

The subfault STFs (B) are related to the observed STFs (D) through a system of equations of the form:

$$D_i(t) = \mathrm{STF}_i(t) = \sum_j^m B_j(t - \tau_{ij}) w_j \qquad (5)$$

where τ is the time delay due to wave and rupture propagation, i is a station index, j is a subfault index and w is a weight proportional to fault slip. In the above system of equations we also impose a positivity constraint to require all subfaults to have the same slip direction. A spatial derivative minimization constraint is applied to smooth the resulting slip model. As a result, Eq. (5) can finally be written in matrix form as:

$$\begin{bmatrix} \mathbf{B} \\ \lambda \mathbf{S} \end{bmatrix} w = \begin{bmatrix} \mathbf{D} \\ 0 \end{bmatrix} \qquad (6)$$

where $\mathbf{S}$ is the matrix of first spatial derivatives and λ (=2) is a constant controlling the weight of the smoothing equation.

The slip weight vector is obtained by standard least squares. Slip amplitudes at each subfault, u_j, are finally obtained based on an independent seismic moment estimate, M_0, through the relation:

$$u_j = \frac{M_0 w_j}{A\mu} \qquad (7)$$

where A is the subfault area and μ is the shear modulus, usually taken equal to 3.5×10^{10} Pa.

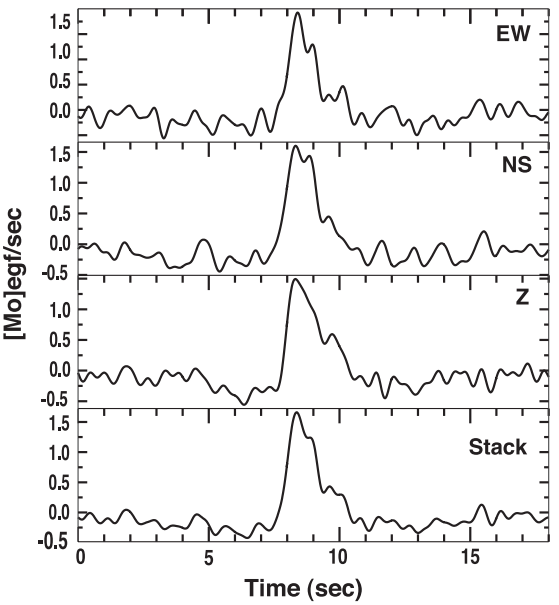

Fig. 5. Example of the source time functions at station ITM derived from deconvolution of the east–west, north–south, and vertical (from top to bottom) eGf waveforms from the corresponding ones of the mainshock. At the lowest part we present the stack of the above three functions, which is finally used in the inversion.

5.2. Application and inversion results

The larger aftershocks of the 2002 Vartholomio sequence, as well as earlier earthquakes of this order of magnitude (3.5–4.5) that occurred near the epicenter of the examined event since the installation of the Greek national broadband network in 1999, were checked to find the optimum event to be used as empirical Green's function. Visual comparison of each event's waveforms with the corresponding waveforms of the mainshock, as well as comparison of their focal mechanisms, wherever possible, was also done. The small event that presented the best similarity with the recorded waveforms of the 2002 Vartholomio mainshock and the best signal to noise ratio, occurred on 30 September 2002 and had a magnitude of M4.1. Its source parameters, as derived from the time domain moment tensor inversion are also included in Table 2.

In Fig. 4, we indicatively compare the horizontal displacement seismograms at the three closest to the epicenter stations for the mainshock and the selected eGf.

The source time functions of the Vartholomio mainshock were estimated using the broadband waveforms from the stations depicted in Fig. 2 with the exception of station KEK, which did not record the eGf. The original data (sampling interval 0.02 s) were integrated to displacement and band-pass filtered in the frequency range 0.05–1.0 Hz. The deconvolution process was performed in the frequency domain, by dividing the displacement spectra of the two events. To avoid instability problems due to spectral sags in the denominator we used a 1% water-level correction (Clayton and Wiggins, 1976). Furthermore, to reduce the noise in the computed source time functions we treated each one of the three-recorded components separately and then stacked the results. An example of the stacking procedure at one of the examined stations is presented in Fig. 5. The final step in the extraction of the STFs included their normalization to unit area.

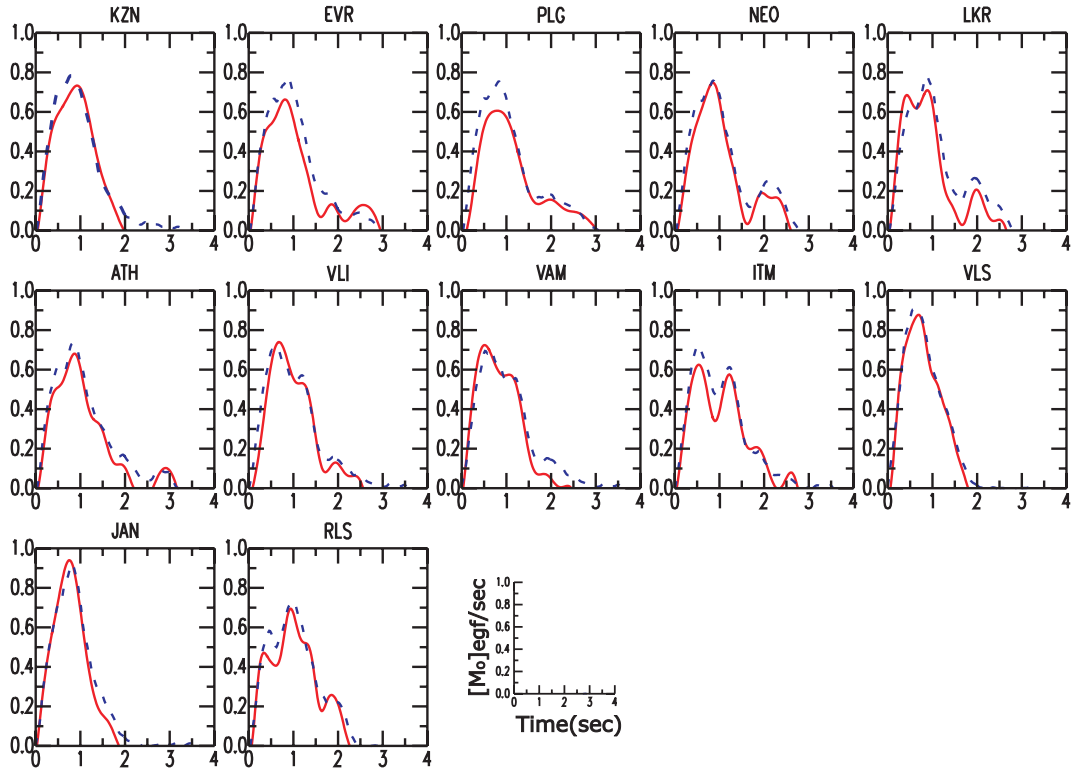

Fig. 6. Observed source time functions (continuous lines) at the 12 examined regional stations are compared with the respective synthetic functions (dashed lines) which correspond to our preferred slip distribution pattern, as depicted in Fig. 7. The name of each station is noted on top of each subplot.

The estimated normalized STFs at the 12 examined stations are presented in Fig. 6. Their shapes do not show any clear implication for unilateral rupture propagation. A careful observer might suggest that if any directivity exists this is towards NW, judging from the slighter shorter durations depicted at stations VLS and JAN.

The fault model employed in the inversion of the STF shapes consists of a planar surface with dimensions 20×20 km, discretized into 0.5 km^2. Regarding the orientation of the plane, the routinely estimated epicenters of the earthquake's sequence do not show a clear trend. Therefore we tested both nodal planes of the mainshock focal mechanism (Fig. 3a) to investigate whether the applied method could statistically identify the one that ruptured, as has been previously done for larger earthquakes (e.g. Dreger, 1994; Antolik, 1996; Roumelioti et al., 2003). Furthermore, we investigated the preferred values for the rupture velocity, V_r and the rise time, τ, which remain fixed during each inversion. Testing different pairs of parameter values performed this investigation and the effectiveness of each pair was evaluated by means of the variance reduction function.

The inversions gave slightly larger variance reduction values (3–4%) for the sinistral NW–SE trending nodal plane, although the difference between the two tested planes cannot be considered significant. Further evidence supporting the NW–SE trending plane as the fault plane comes from the distribution of aftershocks and of the past seismicity of the area, based on advanced relocation techniques. Moreover, the shape

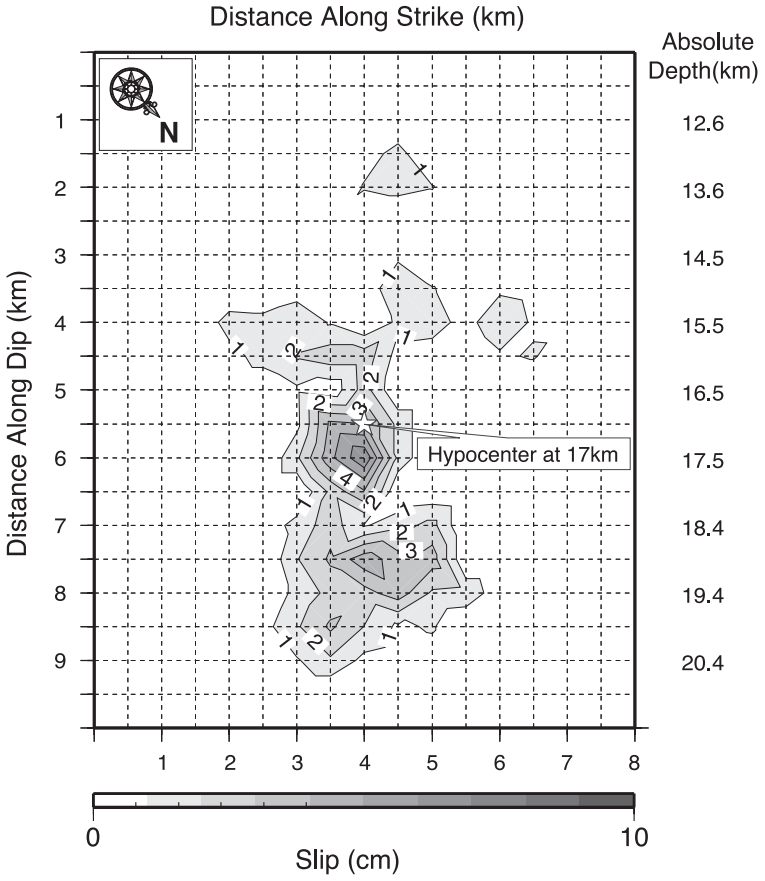

Fig. 7. Slip distribution model for the 2 December 2002, Vartholomio mainshock (**M**5.5). Contours are for 1 cm intervals of slip and white star depicts the adopted hypocentral location. Note that the majority of the slip occurred east of the hypocenter, at greater depths, underneath the western coast of Peloponnese where most of the damage was observed.

of the isoseismals (A. Savaidis, personal communication) also suggests the NW–SE plane as the one that ruptured.

As in the case of the fault plane identification, the resolution in the investigation of the optimum values for the rupture velocity and the rise time was very low. This is probably due to the small dimensions of the examined earthquake source. We could only identify a shallow maximum in variance reduction for τ=0.3–0.4 and V_r=2.4–2.7 km/s. These values are in accordance with those expected from empirical relations (Geller, 1976; Somerville et al., 1999) and do not indicate anything irregular during the source process.

In Fig. 7, we present the slip distribution pattern for our preferred NW–SE trending plane of the Vartholomio mainshock. This model was derived using a value of 0.4 s for the rise time and 2.7 km/s for the rupture velocity and resulted in a variance reduction of the order of 98%. In accordance with the large value of variance reduction, the fit between synthetic and observed STF shapes (Fig. 6) is very satisfactory. Slip weights derived from the STF inversion were scaled using the value of seismic moment (M_0=1.89×10^{17} Nm) estimated from the time domain moment tensor inversion (Fig. 3a). Most of the slip appears to extend within an area of 3.5×5.5 km, concentrated mostly around the hypocenter. The maximum value of slip was estimated to be approximately 7 cm and occurred also close to the hypocenter. It is interesting to note that: (a) even though a directivity might be recognized towards NW, however the major amount of slip is concentrated east of the hypocenter; (b) a significant amount of slip occurs at depths greater than the hypocentral depth, implying that part of the rupture propagated downwards. The projection of this area onto the surface is underneath the western coast of Peloponnese and very close to the town of Vartholomio, which suffered a lot of damage during the earthquake.

6. Conclusions and discussion

Time domain moment tensor inversion was used to investigate the source characteristics of the Vartholomio earthquake of 2 December 2002 (GMT 04:58:56, 37.83°N; 21.12°E), and of three of its larger aftershocks. The focal mechanisms (Fig. 8) show almost

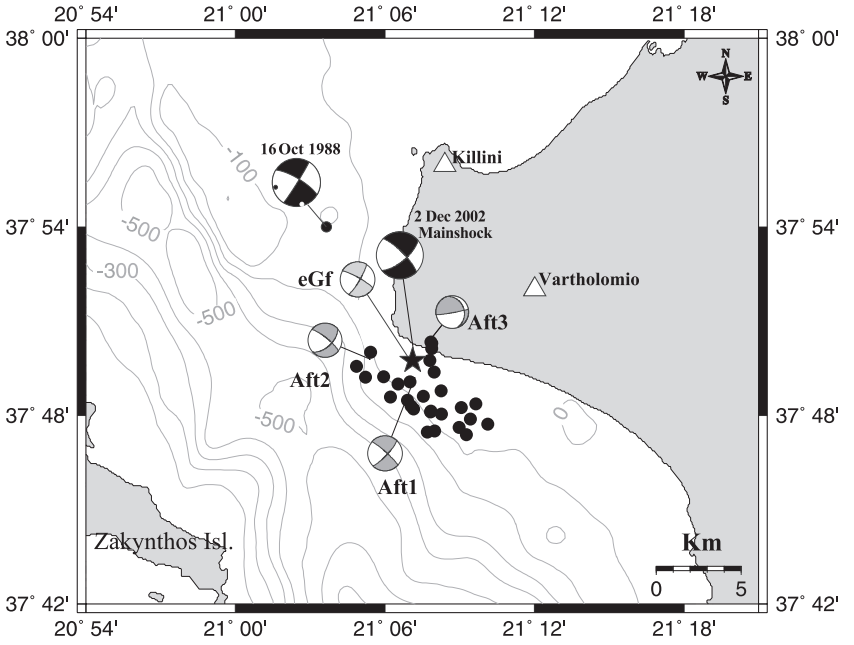

Fig. 8. Map of the studied area showing preliminary relocated epicenters of the 2002 Vartholomio sequence and focal mechanisms estimated in the present study. The star corresponds to the mainshock epicenter. The focal mechanism of the 16 October 1988 earthquake is also shown for comparison.

pure strike slip faulting, in accordance with previous studies (Papazachos et al., 1998; Kiratzi and Louvari, 2003). The largest previous earthquake occurred on 16 October 1988 and exhibited strike-slip faulting, as well (Fig. 8).

We also investigated the slip distribution of the mainshock, by combining an empirical Green's function approach and a source time function shape inversion scheme. The dimensions of the ruptured area were estimated to be 3.5×5.5 km and considering a hypocentral depth of 17 km, the slip did not reach the surface but stopped at a depth of about 12 km. No clear directivity was detected, only weak indication for directivity towards NW from the shape of the STFs. The slip distribution model of the Vartholomio mainshock indicates significant slip, at relatively large depths beneath the earthquake's hypocenter. This area of major slip is underneath the coast of western Peloponnese and very close to the town of Vartholomio where most of the damage was observed.

Finally, our efforts to statistically discriminate the fault plane of the mainshock did not yield safe results. There is indication that the NW–SE trending plane is the fault plane, which is connected with sinistral strike-slip motion. This gave larger values of variance reduction in all our inversion tests, although this result was found to be statistically insignificant. Nevertheless, the distribution of relocated epicentres of the sequence (Fig. 8) and preliminary analysis of macroseismic data also favor the NW–SW trending plane. Another interesting feature is the occurrence of off-fault aftershocks that exhibit a nearly N–S trend, and the focal mechanism of one of the larger aftershocks (Aft3 in Fig. 8), which has a nodal plane that is compatible with this trend. A careful investigation of these patterns, as well as kinematic implications for the broader area will be the target of future work, after all data become available.

Acknowledgements

Moment tensors were computed using the mtpackagev1.1 package developed by Douglas Dreger of the Berkeley Seismological Laboratory, and Green's functions were computed using the FKRPROG software developed by Chandan Saikia of URS. This work was financially supported by the General Secretariat of Research and Technology (GSRT) of the Ministry of Development of Greece.

References

Antolik, M.S., 1996. New results from studies of three outstanding problems in local, regional and global seismology, PhD thesis. University of California, Berkeley, 311 pp.

Benetatos, Ch., Roumelioti, Z., Kiratzi, A., Melis, N., 2002. Source parameters of the *M* 6.5 Skyros Island (North Aegean Sea) earthquake of July 26, 2001. Ann. Geophys. 45 (3/4), 513–526.

Benetatos, Ch., Kiratzi, A., Roumelioti, Z., Stavrakakis, G., Drakatos, G., Latoussakis, I., 2004. The 14 August 2003 Lefkada Island (Greece) earthquake: focal mechanisms of the mainshock and of the aftershock sequence. J. Seismol. (submitted for publication).

Clayton, R.W., Wiggins, R.A., 1976. Source shape estimation and deconvolution of teleseismic body waves. Geophys. J. R. Astron. Soc. 47, 151–177.

Dreger, D.S., 1994. Empirical Green's function study of the January 17, 1994 Northridge, California earthquake. Geophys. Res. Lett. 21, 2633–2636.

Dreger, D.S., 2002. Manual of the Time-Domain Moment Tensor Inverse Code (TDMT_INVC), Release 1.1. Berkeley Seismological Laboratory, Berkeley, CA, pp. 18.

Dreger, D.S., Helmberger, D.V., 1990. Broadband modeling of local earthquakes. Bull. Seismol. Soc. Am. 80, 1162–1179.

Dreger, D.S., Helmberger, D.V., 1991. Complex faulting deduced from broadband modelling of the 28 February 1990 Upland earthquake (M_L=5.2). Bull. Seismol. Soc. Am. 81, 1129–1144.

Dreger, D.S., Helmberger, D.V., 1993. Determination of source parameters at regional distances with single station or sparse network data. J. Geophys. Res. 98, 8107–8125.

Geller, R.J., 1976. Scaling relations for earthquake source parameters and magnitudes. Bull. Seismol. Soc. Am. 66, 1501–1523.

Hartzell, S.H., 1978. Earthquake aftershocks as Green's functions. Geophys. Res. Lett. 5 (1), 1–4.

Jost, M.L., Herrmann, R., 1989. A student's guide to and review of moment tensors. Seismol. Res. Lett. 60, 37–57.

Kiratzi, A., Louvari, E., 2003. Focal mechanisms of shallow earthquakes in the Aegean Sea and the surrounding lands determined by waveform modeling: a new database. J. Geodyn. 36, 251–274.

Le Pichon, X., Chamot-Rooke, N., Lallemant, S., Noomen, R., Veis, G., 1995. Geodetic determination of the kinematics of central Greece with respect to Europe: implications for eastern Mediterranean tectonics. J. Geophys. Res. 100, 12675–12690.

Louvari, E., Kiratzi, A.A., Papazachos, B.C., 1999. The Cephalonia transform fault and its extension to western Lefkada island. Tectonophysics 308, 223–236.

McClusky, S., Balassanian, S.S., Barka, A., Demir, C., Georgiev, S.E.I., Gurkan, O., Hamburger, M., Hurst, K., Kahle, H.,

Kastens, K., Kekelidze, G., King, R., Kotzev, V., Lenk, O., Mahmoud, S., Mishin, A., Nadariya, M., Ouzounis, A., Paradisis, D., Peter, Y., Prilepin, M., Reilinger, R., Sanli, I., Seeger, H., Tealeb, A., Toksöz, M.N., Veis, G., 2000. Global positioning system constraints on plate kinematics and dynamics in the eastern Mediterranean and Caucasus. J. Geophys. Res. 105, 5695–5719.

McKenzie, D.P., 1972. Active tectonics of the Mediterranean sea. Geophys. J.R. Astron. Soc. 30, 109–185.

Mori, J., Hartzell, S., 1990. Source inversion of the 1988 Upland earthquake: determination of a fault plane for a small event. Bull. Seismol. Soc. Am. 80, 278–295.

Panagiotopoulos, D.G., Hatzidimitriou, P.M., Karakaisis, G.F., Papadimitriou, E.E., Papazachos, B.C., 1985. Travel time residuals in southeastern Europe. PAGEOPH 123, 221–231.

Papadopoulos, G.A., Karastathis, V.K., Ganas, A., Pavlides, S., Fokaefs, A., Orfanogiannaki, K., 2003. The Lefkada, Ionian sea (Greece), shock (*Mw* 6.2) of 14 August 2003: evidence for the characteristic earthquake from seismicity and ground failures. Earth Planets Space 55, 713–718.

Papazachos, B.C., Papadimitriou, E.E., Kiratzi, A.A., Papazachos, C.B., Louvari, E.K., 1998. Fault plane solutions in the Aegean Sea and the surrounding area and their tectonic implication. Boll. Geofis. Teor. Appl. 39, 199–218.

Pasyanos, M.E., Dreger, D.S., Romanowicz, B., 1996. Towards real-time determination of regional moment tensors. Bull. Seismol. Soc. Am. 86, 1255–1269.

Roumelioti, Z., Kiratzi, A., Dreger, D., 2003. The source process of the July 26, 2001 Skyros island (Greece) earthquake. Geophys. J. Int. 156 (3), 541–548.

Saikia, C.K., 1994. Modified frequency-wavenumber algorithm for regional seismograms using Filon's quadrature; modelling of Lg waves in eastern North America. Geophys. J. Int. 118, 142–158.

Somerville, P., Irikura, K., Graves, R., Sawada, S., Wald, D., Abrahamson, N., Iwasaki, Y., Kagawa, T., Smith, N., Kowada, A., 1999. Characterizing crustal earthquake slip models for the prediction of strong ground motion. Seismol. Res. Lett. 70, 59–80.

Tselentis, G.-A., Zahradnik, J., 2000. The Athens earthquake of 7 September 1999. Bull. Seismol. Soc. Am. 90, 1143–1160.

Waldhauser, F., Ellsworth, W.L., 2000. A double-difference earthquake location algorithm: method and application to the Northern Hayward fault, California. Bull. Seismol. Soc. Am. 90, 1353–1368.

Zahradnik, J., 2001. Modelling the Skyros island, Aegean Sea M_w=6.5 earthquake of July 26, 2001. Research Report. Faculty of Mathematics and Physics, Charles University, Prague. (http://www.seis30.karlov.mff.cuni.cz).